

Analysis of heat and mass transport characteristics in microchannel reactors with non-uniform catalyst distributions for hydrogen production

Shian Li, Zhi Yang, Yihui Liu, Qiuwan Shen and Guogang Yang
Dalian Maritime University, Dalian, China, and

Bengt Ake Sunden
Department of Energy Sciences, Lund University, Lund, Sweden

Heat and mass
transport
characteristics

3191

Received 8 December 2021
Revised 29 December 2021
4 January 2022
5 January 2022
Accepted 5 January 2022

Abstract

Purpose – The purpose of this paper is to investigate the heat and mass transport characteristics in microchannel reactors with non-uniform catalyst distributions.

Design/methodology/approach – A two-dimensional model is developed to study the heat and mass transport characteristics in microchannel reactors. The heat and mass transport processes in the microchannel reactors with non-uniform catalyst distribution in the catalytic combustion channel are also studied.

Findings – The simulated results are compared in terms of the distributions of species mole fraction, temperature and reaction rate for the conventional and new designed reactors. It is found that the chemical reaction, heat and mass transport processes are significantly affected and the maximum temperature in the reactor is also greatly reduced when a non-uniform catalyst distribution is applied in the combustion catalyst layer.

Practical implications – This study can improve the understanding of the transportation characteristics in microchannel reactors with non-uniform catalyst distributions and provide guidance for the design of microchannel reactors.

Originality/value – The design of microchannel reactors with non-uniform catalyst distributions can be used in methane steam reforming to reduce the maximum temperature inside the reactor.

Keywords Temperature distribution, Catalyst distribution, Methane steam reforming, Microchannel reactor

Paper type Research paper

© Shian Li, Zhi Yang, Yihui Liu, Qiuwan Shen, Guogang Yang and Bengt Ake Sunden. Published by Emerald Publishing Limited. This article is published under the Creative Commons Attribution (CC BY 4.0) licence. Anyone may reproduce, distribute, translate and create derivative works of this article (for both commercial and non-commercial purposes), subject to full attribution to the original publication and authors. The full terms of this licence may be seen at <http://creativecommons.org/licenses/by/4.0/legalcode>

Funding: Dalian City Innovative Support Program for High-Level Talents (No. 2019RQ036). China Postdoctoral Science Foundation (No. 2019M651097 and No. 2019M651094). Natural Science Foundation of Liaoning Province (No. 2020-HYLH-38). National Natural Science Foundation of China (52001045).



Nomenclature

A = coefficient;
 c_p = specific heat, $\text{J kg}^{-1} \text{K}^{-1}$;
 d = diameter, m;
 D = diffusivity, $\text{m}^2 \text{s}^{-1}$;
 E = Activation energy, J mol^{-1} ;
 h = enthalpy, J mol^{-1} ;
 k = thermal conductivity, $\text{W m}^{-1} \text{K}^{-1}$;
 K = permeability, m^2 ;
 M = molecular weight, kg mol^{-1} ;
 P = pressure, Pa;
 R = universal gas constant, $8.314 \text{ J mol}^{-1} \text{K}^{-1}$;
 R_i = reaction rate, $\text{mol m}^{-3} \text{s}^{-1}$;
 S = source term;
 T = temperature, K;
 \vec{u} = velocity vector, m/s;
 X = Mole fraction; and
 Y = mass fraction.

Greek symbols

α = coefficient;
 ε = porosity;
 μ = dynamic viscosity, Pa s;
 ρ = density, kg m^{-3} ; and
 τ = tortuosity.

Superscripts and subscripts

eff = effective;
f = fluid;
i = *i*th species;
k = Knudsen;
m = mixture;
mass = mass equation;
mom = momentum equation;
p = pore;
s = solid; and
T = temperature equation.

1. Introduction

Hydrogen is commonly used as the ideal fuel for fuel cells (Chen *et al.*, 2020; Li *et al.*, 2017; Li and Sunden, 2018; Li *et al.*, 2021; Mauro *et al.*, 2010; Peng *et al.*, 2020; Shen *et al.*, 2019). Various methods have been developed to produce hydrogen from methane, such as steam reforming, partial oxidation and autothermal reforming (Yuan *et al.*, 2007). Methane steam reforming can be used for hydrogen production. For the methane steam reforming, an external heat source must be supplied to maintain the hydrogen production process due to the endothermic reaction. Microchannel reactors with both a reforming channel and a catalytic combustion channel have superior heat transfer characteristics (Bhat and Sadhukhan, 2009). The exothermic reaction in the combustion channel can act as the heat source for the reactions in the reforming channel.

Many numerical studies have already been carried out for methane steam reforming in microchannel reactors. The chemical reaction coupled mass and heat transport phenomena in a methane reformer duct were analyzed by [Yuan *et al.* \(2007\)](#). It was concluded that the porous layer configuration, temperature and catalyst loading have strong effects on the transport processes and reformer performance. In addition, a similar study was carried out by [Ni \(2013\)](#). Effects of pore size, permeability, gas velocity, temperature and rate of heat supply on the reformer performance were systematically discussed. The reforming channel is considered in the above-mentioned numerical simulations and a constant heat flux is applied as the heat source.

The thermal characteristics of a microchannel reactor with co-flow and counter-flow arrangements were numerically investigated by [Zanfir and Gavriilidis \(2004\)](#). It was found that the thermal behavior was strongly affected by the flow arrangements. The reactor is better balanced thermally for the co-flow arrangement compared with a counter-flow arrangement. Effects of inlet parameters of the reforming flow channel and the combustion flow channel on the reactor performance were systematically studied using a mathematical model by [Wang *et al.* \(2012\)](#). Results showed that a hot spot near the reactor inlet was observed due to the local imbalance of the heating effect of steam reforming and catalytic combustion in the corresponding channels. A microchannel reactor for methane steam reforming with a stripe combustion catalyst layer was suggested to minimize the hot spot by [Jeon *et al.* \(2013\)](#). The response surface methodology was used to obtain the optimal optimize stripe configuration. It was concluded that the stripe combustion catalyst layer can greatly decrease the maximum temperature without any methane conversion loss. Methane steam reformers with three different wall-coated catalyst layer patterns were presented, and the corresponding thermal behavior and the reaction kinetics were analyzed by [Settar *et al.* \(2015\)](#). Recently, the effect of discrete catalytic layer arrangement on methane steam reforming performance has been studied by [Wang *et al.* \(2021\)](#). The heat and mass transport processes inside different reactors were investigated and compared in detail. Segmented and continuously coated catalyst layers were applied in microchannel reactors for methane steam reforming by [Mundhwa and Thurgood \(2017\)](#). Different combinations of segmented and continuous configurations are used to examine the heat, mass and chemical reaction processes. The maximum temperature, thermal hot spots and axial thermal gradients were significantly decreased when the segmented configurations were adopted in the reactors.

The formation of a hot spot in the reactor can result to material failure and catalyst deactivation ([Bartholomew, 2001](#)). To reduce the maximum temperature in the reactor, a non-uniform catalyst distribution is proposed in the catalytic combustion channel. In this study, a two-dimensional mathematical model was developed and applied to study the heat and mass transport processes in the microchannel reactors with non-uniform catalyst distribution in the catalytic combustion channel. This approach forms a unique and novel investigation of significant relevance for hydrogen production. This non-uniform catalyst distribution is used in the catalytic combustion channel of microchannel reactors for the first time.

2. Model description

2.1 Physical model

[Figure 1](#) presents the schematic of a microchannel reactor for hydrogen production. The computational domain consists of several layers, i.e. the reforming channel, reforming catalyst layer, the combustion channel, the combustion catalyst layer and the solid plate. The reactor length is 50 mm, the channel height is 0.5 mm, and the catalyst layer thickness is 0.1 mm. The thickness of the solid plate in the middle is 0.5 mm, and the thickness of the top

and bottom solid plates is 0.25 mm. A co-flow arrangement is adopted in the microchannel reactor. The detailed information can be found in Table 1. The thermal conductivities of catalyst layer and solid plate provided by Jeon *et al.* (2013) were used in this study.

In this study, a non-uniform catalyst distribution is applied in the combustion catalyst layer. It is assumed that the catalytic combustion rate is proportional to the catalyst loading. The catalytic combustion rate is multiplied by a coefficient for the implementation of uniform and non-uniform catalyst distributions. The catalytic combustion rate is described in the following section. This coefficient is labeled as α . Four cases are considered in this study. For Case A, a uniform catalyst distribution is studied. For Case B, a non-uniform catalyst distribution (α varies from 0.25 to 1.75) is applied. For Case C, a non-uniform catalyst distribution (α varies from 0.5 to 1.5) is considered. For Case D, a non-uniform catalyst distribution (α varies from 0.75 to 1.25) is investigated. The profiles of the coefficient α distribution in the four cases are plotted in Figure 2. The maximum slope of the profile is provided by Case B and followed by Case C, Case D and Case A.

2.2 Governing equations

The mass, momentum, species and energy equations are solved to describe the methane steam reforming and catalytic combustion processes in microchannel reactors.

Mass equation:

$$\nabla \cdot (\rho \vec{u}) = S_{mass} \tag{1}$$

where S_{mass} is the source term.

Momentum equation:

Figure 1.
Schematic of a microchannel reactor for hydrogen production

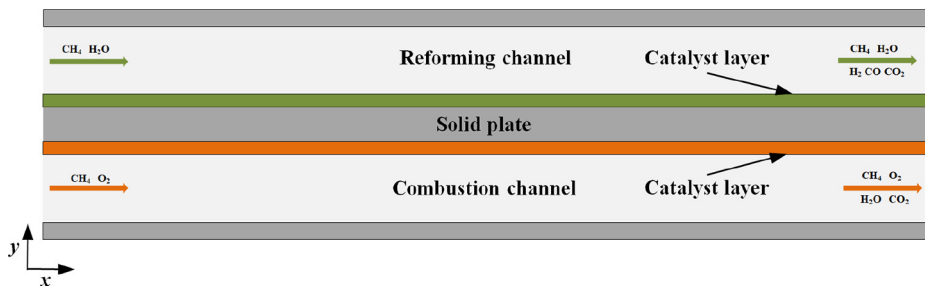


Table 1.
Geometric and physical parameters

Parameter	Value	Unit
Channel length	50	mm
Channel height	0.5	mm
Catalyst layer thickness	0.1	mm
Solid plate thickness	0.5/0.25	mm
Catalyst layer porosity	0.5	
Catalyst layer tortuosity	4	
Catalyst layer pore diameter	300	nm
Catalyst layer thermal conductivity	2	W m ⁻¹ K ⁻¹
Solid plate thermal conductivity	20	W m ⁻¹ K ⁻¹

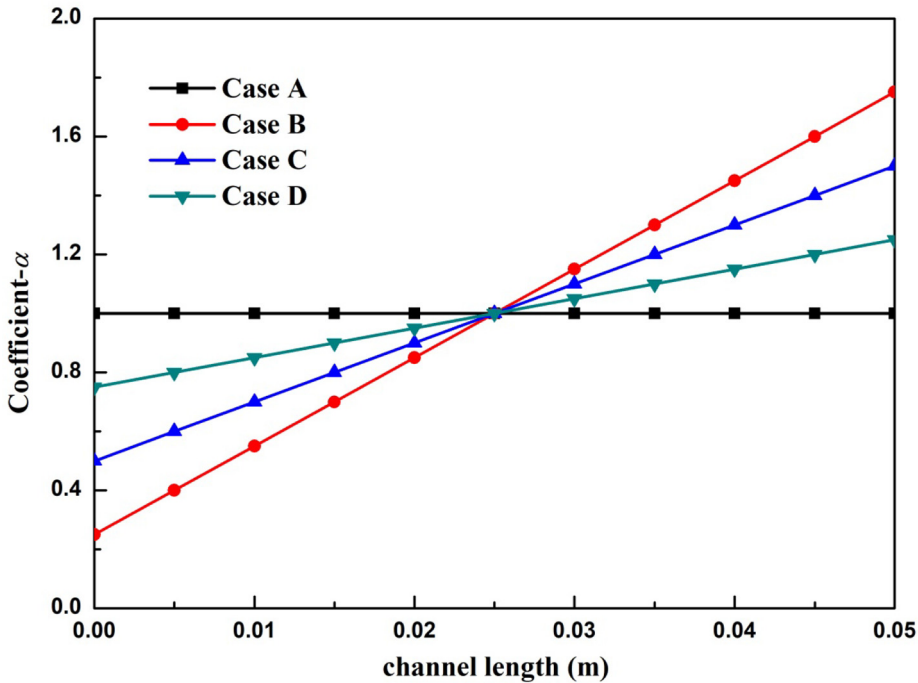


Figure 2. The profiles of the coefficient α distribution in the four cases

$$\nabla \cdot (\rho \vec{u} \vec{u}') = \nabla \cdot (\mu \nabla \vec{u}') - \nabla P + S_{mom} \quad (2)$$

where S_{mom} is the source term. In the porous layers, the Darcy's law is adopted [9].
Species equation:

$$\nabla \cdot (\rho \vec{u} Y_i) = \nabla \cdot (\rho D_{eff,i} \nabla Y_i) + S_i \quad (3)$$

where S_i is the source term caused by the chemical reactions.

Energy equation:

$$\nabla \cdot (\rho c_p \vec{u} T) = \nabla \cdot (k_{eff} \nabla T) + S_T \quad (4)$$

where S_T is the generated or consumed heat by the corresponding reactions.

Hydrogen is produced in the reforming catalyst layer and heat is generated in the combustion catalyst layer. The methane steam reforming is accompanied by the water-gas shift reaction and reverse methanation reaction. The corresponding reactions are as follows:

Methane steam reforming reaction



Water-gas shift reaction



Reverse methanation reaction



Catalytic combustion of methane



The kinetic rate equations developed by [Xu and Froment \(1989\)](#) was used in the reforming catalyst layer.

$$R_1 = Bk_1/p_{\text{H}_2}^{2.5} \left(p_{\text{CH}_4} p_{\text{H}_2\text{O}} - p_{\text{H}_2}^3 p_{\text{CO}} / K_{e,1} \right) / \text{DEN}^2 \quad (9)$$

$$R_2 = Bk_2/p_{\text{H}_2} \left(p_{\text{CO}} p_{\text{H}_2\text{O}} - p_{\text{H}_2} p_{\text{CO}_2} / K_{e,2} \right) / \text{DEN}^2 \quad (10)$$

$$R_3 = Bk_3/p_{\text{H}_2}^{3.5} \left(p_{\text{CH}_4} p_{\text{H}_2\text{O}}^2 - p_{\text{H}_2}^4 p_{\text{CO}_2} / K_{e,3} \right) / \text{DEN}^2 \quad (11)$$

$$\text{DEN} = 1 + K_{\text{CO}} p_{\text{CO}} + K_{\text{H}_2} p_{\text{H}_2} + K_{\text{CH}_4} p_{\text{CH}_4} + K_{\text{H}_2\text{O}} p_{\text{H}_2\text{O}} / p_{\text{H}_2} \quad (12)$$

In the above equations, k_j is the reaction constant, p_i is the partial pressure of i th species, $K_{e,j}$ is the equilibrium reaction constant, and K_i is the adsorption constant of i th species. The coefficient B is used to convert the unit of reaction rate from $\text{kmol}/(\text{kg}_{\text{cat}} \text{h})$ to $\text{mol}/(\text{m}^3 \text{s})$ ([Sohn et al., 2016](#)).

The reaction kinetics proposed by [Song et al. \(1991\)](#) was applied for the catalytic combustion of methane.

$$R_4 = C \exp(-E/RT) X_{\text{CH}_4} X_{\text{O}_2}^{0.5} \quad (13)$$

where X_i is the mole fraction, C is the coefficient, E is the activation energy.

The source terms of the governing equations and the parameters in the kinetic rate equations are given in [Tables 2 and 3](#) ([Zanfir and Gavrilidis, 2003](#); [Elnashaie et al., 1990](#)).

2.3 Numerical implementation

The commercial software ANSYS FLUENT is used for the development of mathematical model. The chemical reaction rate, mass diffusivity and source terms are implemented by using the user defined functions (UDFs). The detailed descriptions of boundary conditions can be found in [Table 4](#). The pressure and velocity fields are linked by the SIMPLE algorithm. As shown in [Figure 3](#), three mesh systems ($x \times y$), namely, mesh I (100×48), mesh II (150×60) and mesh III (200×72), are used for the mesh independence study. And the mesh system of 150×60 is used for the numerical simulations.

Description	Units
$S_{mass} = S_{CH_4} + S_{H_2O} + S_{CO} + S_{CO_2} + S_{H_2}$ (reforming catalyst layer)	$\text{kg m}^{-3} \text{s}^{-1}$
$S_{mass} = S_{CH_4} + S_{O_2} + S_{CO_2} + S_{H_2O}$ (combustion catalyst layer)	$\text{kg m}^{-3} \text{s}^{-1}$
$S_{mom} = -\frac{\mu}{K} \vec{u}$ (reforming/combustion catalyst layer)	$\text{kg m}^{-2} \text{s}^{-2}$
$S_{CH_4} = (-R_1 - R_3)M_{CH_4}$ (reforming catalyst layer)	$\text{kg m}^{-3} \text{s}^{-1}$
$S_{H_2O} = (-R_1 - R_2 - 2R_3)M_{H_2O}$ (reforming catalyst layer)	$\text{kg m}^{-3} \text{s}^{-1}$
$S_{CO} = (R_1 - R_2)M_{CO}$ (reforming catalyst layer)	$\text{kg m}^{-3} \text{s}^{-1}$
$S_{CO_2} = (R_2 + R_3)M_{CO_2}$ (reforming catalyst layer)	$\text{kg m}^{-3} \text{s}^{-1}$
$S_{H_2} = (3R_1 + R_2 + 4R_3)M_{H_2}$ (reforming catalyst layer)	$\text{kg m}^{-3} \text{s}^{-1}$
$S_{CH_4} = -R_4M_{CH_4}$ (combustion catalyst layer)	$\text{kg m}^{-3} \text{s}^{-1}$
$S_{O_2} = -2R_4$ (combustion catalyst layer)	$\text{kg m}^{-3} \text{s}^{-1}$
$S_{CO_2} = R_4M_{CO_2}$ (combustion catalyst layer)	$\text{kg m}^{-3} \text{s}^{-1}$
$S_{H_2O} = 2R_4M_{H_2O}$ (combustion catalyst layer)	$\text{kg m}^{-3} \text{s}^{-1}$
$S_T = \sum_i R_i \Delta h_{reaction,i}$ (reforming/combustion catalyst layer)	W m^{-3}

Table 2.

Source terms of the governing equations

Description	
Effective mass diffusivity	$D_{eff,i} = \frac{\varepsilon}{\tau} \times \frac{D_{i,m} \times D_{i,k}}{D_{i,m} + D_{i,k}}$
Effective thermal conductivity	$k_{eff} = (1 - \varepsilon)k_s + \varepsilon k_f$
Kinetic rate constant	$k_1 = 4.225 \times 10^{15} \times e^{(-240100/RT)}$
Kinetic rate constant	$k_2 = 1.955 \times 10^6 \times e^{(-67130/RT)}$
Kinetic rate constant	$k_3 = 1.02 \times 10^{15} \times e^{(-243900/RT)}$
Equilibrium constant	$k_{e,1} = 5.75 \times 10^{12} \times e^{(-11476/RT)}$
Equilibrium constant	$k_{e,2} = 1.26 \times 10^{-2} \times e^{(4639/RT)}$
Equilibrium constant	$k_{e,3} = 7.24 \times 10^{10} \times e^{(-21646/RT)}$
Adsorption constant	$K_{CH_4} = 6.65 \times 10^{-4} \times e^{(-38280/RT)}$
Adsorption constant	$K_{CO} = 8.23 \times 10^{-5} \times e^{(-70650/RT)}$
Adsorption constant	$K_{H_2} = 6.12 \times 10^{-4-9} \times e^{(-82900/RT)}$
Adsorption constant	$K_{H_2O} = 1.77 \times 10^5 \times e^{(88680/RT)}$

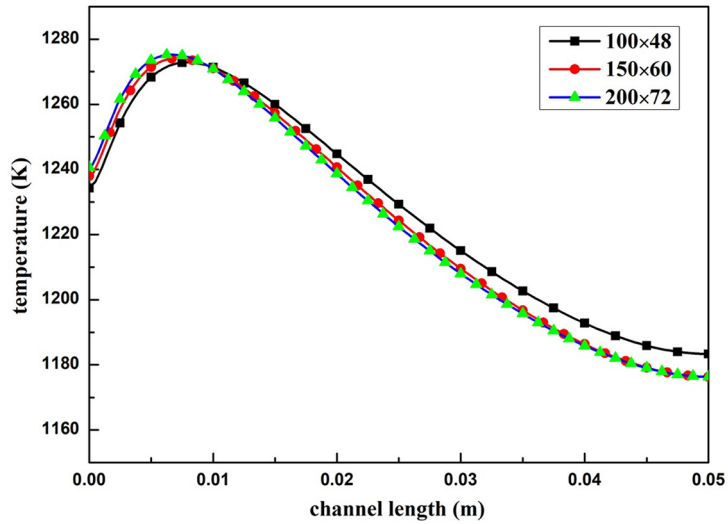
Table 3.

Complementary expressions

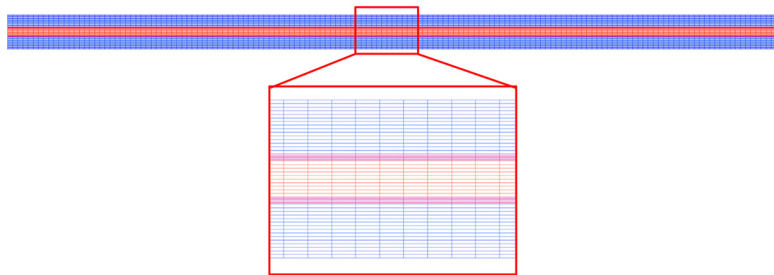
Description	Conditions	Value	Units
Reforming channel inlet	Velocity	4	m/s
	Mole fraction	$\text{CH}_4:\text{H}_2\text{O} = 0.75:0.25$	-
	Temperature	1073	K
Combustion channel inlet	Velocity	3	m/s
	Mole fraction	$\text{CH}_4:\text{Air} = 0.09:0.91$	-
Reforming channel outlet	Temperature	1073	K
	Pressure	0	Pa
Combustion channel outlet	Pressure	0	Pa

Table 4.

Boundary conditions



(a)



(b)

Figure 3.
Mesh independence
study

Notes: (a) temperature distributions at the middle of the solid plate of three mesh systems; (b) the mesh used in this study

3. Results and discussion

Model validation was carried out to assess the accuracy of the mathematical model. This was done by comparing computational results with available experimental data. The same configuration and operating conditions were adopted in the numerical simulations. The methane conversion rates for temperatures varying from 923 to 1123 K were predicted. As shown in Figure 4, the numerical results agree well with the experimental data provided by Irani *et al.* (2011).

Figure 4 shows the mole fractions of the four cases in the reforming channel and at the catalyst layer interface. As seen in Figure 5(a), the methane mole fraction is gradually decreased along the flow direction. This is attributed to the reactions of the methane steam reforming and reverse methanation. It can be observed in Figure 5(b) that the hydrogen mole

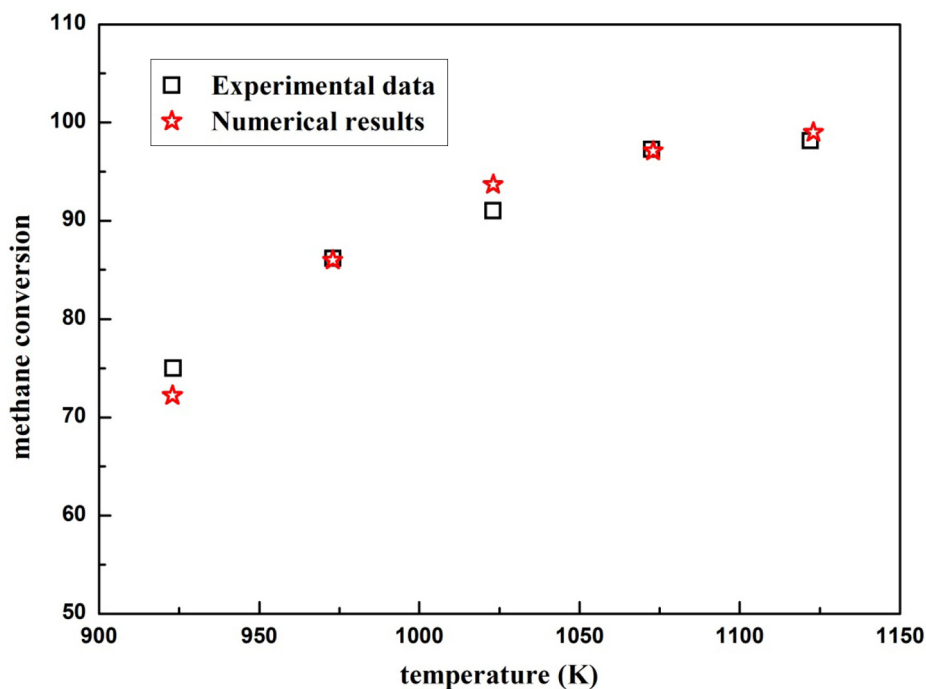


Figure 4.
Comparison between
the numerical results
and experimental
data

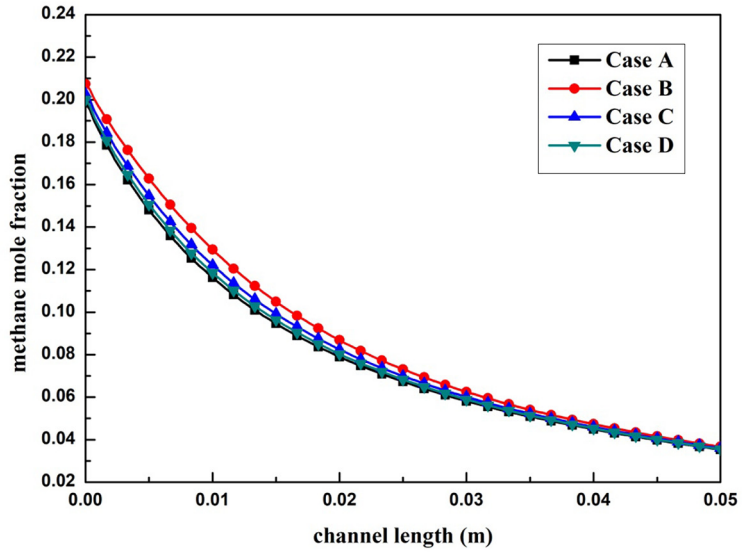
fraction is gradually increased along the flow direction due to the reactions of the methane steam reforming, water-gas shift reaction and the reverse methanation. The methane conversion rates for the four cases are 78.35, 77.44, 77.96 and 78.21%, respectively. This reveals that the application of a non-uniform catalyst distribution in the combustion catalyst layer has a slight effect on the methane conversion rate.

The profiles of methane mole fraction of four cases in the combustion channel and catalyst layer interface are plotted in Figure 6. The methane is gradually consumed by the catalytic combustion reaction which is an exothermic process. And the generated heat is transferred to the reforming side for the methane steam reforming reactions through the solid plate in the middle. It also can be seen that methane is almost consumed by the catalytic combustion reaction.

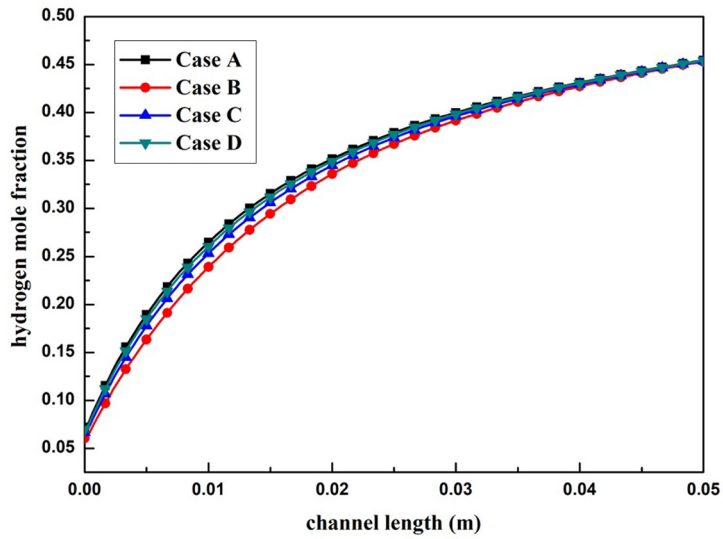
The temperature distributions of the four cases are presented in Figure 7. It is clearly seen that the temperature is gradually increased and then decreased. In addition, the local temperature distributions at the middle of the solid plate are presented in Figure 8. For Case A, the temperature is increased from 1237.9 to 1274.1 K and then decreased to 1176.3 K. For Case B, the temperature is increased from 1150.8 to 1242.8 K and then decreased to 1190.5 K. For Case C, the temperature is increased from 1196.0 to 1253.3 K and then decreased to 1183.3 K. For Case D, the temperature is increased from 1221.2 to 1264.5 K and then decreased to 1179.2 K. It is obvious that the maximum temperature is decreased when a non-uniform catalyst distribution is applied in the combustion catalyst layer. In addition, the location of the maximum temperature is also significantly affected by the distribution of the catalyst. Case B provides the best performance in terms of attaining more uniform temperature profile.

HFF
32,10

3200



(a)



(b)

Figure 5.
Mole fractions in the
reforming channel
and catalyst layer
interface

Notes: (a) Methane mole fraction; (b) hydrogen mole fraction

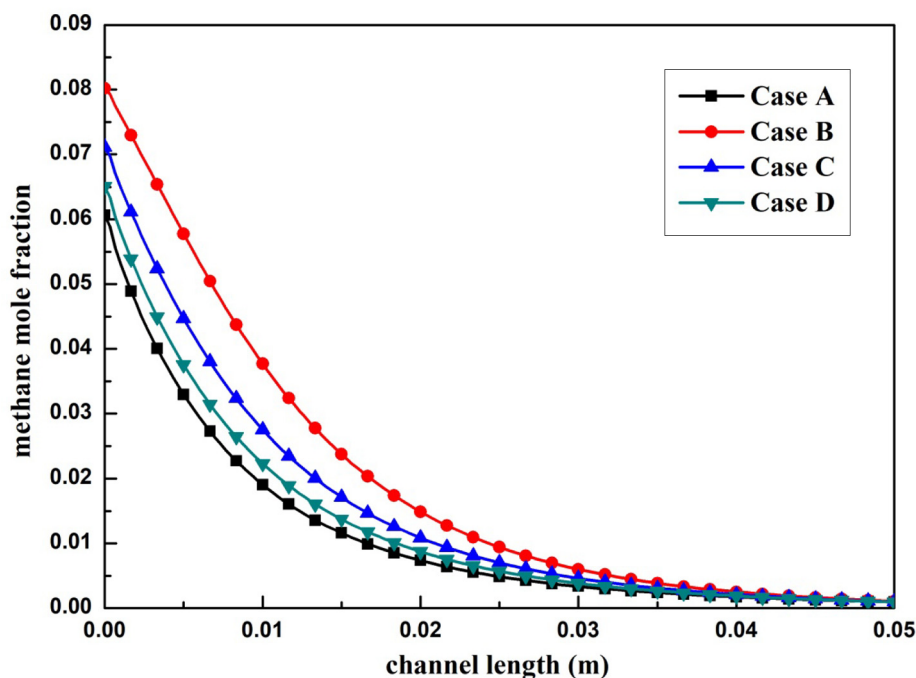


Figure 6.
Methane mole
fraction in the
combustion channel
and catalyst layer
interface

The steam reforming reaction rate distributions in the reforming catalyst layer are given in Figure 9. It can be seen that the reaction rate is gradually decreased due to the consumption of methane and water. Also, the reaction rate is decreased from the reforming channel-catalyst layer interface to the catalyst layer- solid plate interface because the mass transport resistance in the porous regions. In addition, the local profiles of the steam reforming reaction rate of the four cases at the middle of the reforming catalyst layer are exhibited in Figure 10. It is evident that the reaction rate is significantly affected by the distributions of the catalyst upstream of the catalyst layer. The corresponding maximum reaction rates of four cases are 2292.6, 1689.3, 1990.4 and 2170.0 mol/(m³ s), respectively.

The water-gas shift reaction rate distributions in the reforming catalyst layer of the four cases are shown in Figure 11. The maximum reaction rate appears near the outlet region and the minimum reaction rate appears near the inlet region. The local profiles of the water-gas shift reaction rate of four cases at the middle of the reforming catalyst layer are shown in Figure 12. The reaction rate is gradually increased along the flow direction. Also, the reaction rate is greatly influenced by the distributions of the catalyst, especially downstream of the catalyst layer. The corresponding maximum reaction rates of four cases are 2.7, 2.2, 2.4 and 2.6 mol/(m³ s), respectively.

The distributions of the reverse methanation reaction rate in the reforming catalyst layer of the four cases are shown in Figure 13. The local profiles of the reverse methanation reaction rate of the four cases at the middle of the reforming catalyst layer are illustrated in Figure 14. It is obvious that the reaction rate is sharply decreased close to the inlet region

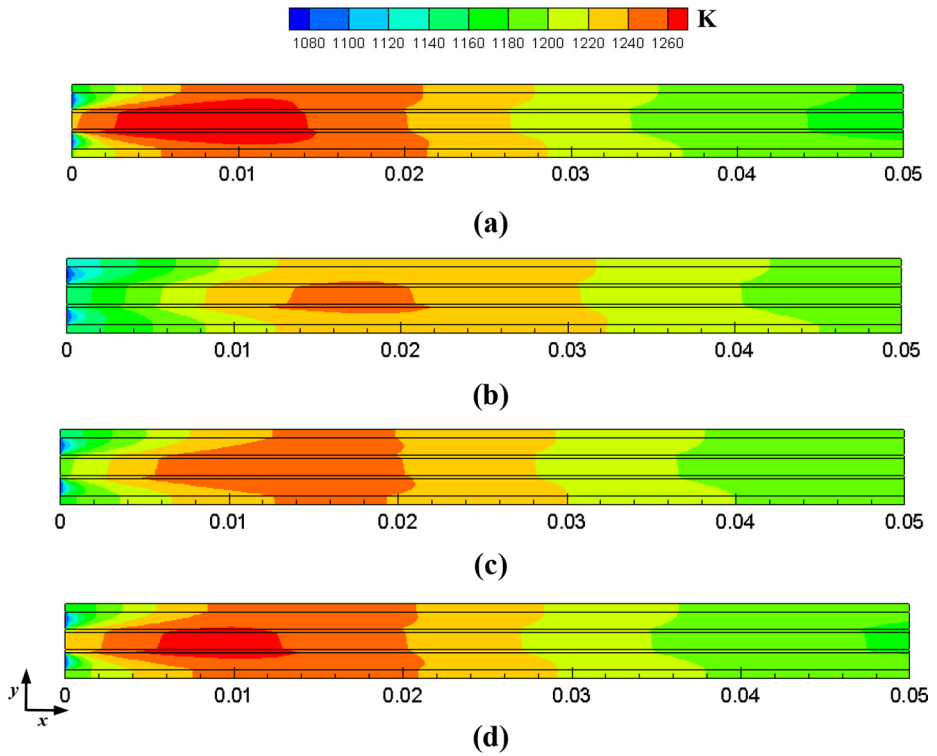


Figure 7.
The temperature
distributions of the
four cases

Notes: (a) CaseA; (b) Case B; (c) Case C; (d) Case D

and then gradually decreases. The profiles of the four cases are also similar while the maximum reaction rates are different. The corresponding reaction rates are 3117.7, 2720.6, 2925.2 and 3041.0 mol/(m³ s), respectively.

The catalytic combustion reaction rate distributions in the combustion catalyst layer of the four cases are shown in Figure 15. It can be seen that the maximum reaction rate appears near the inlet region and the minimum reaction rate appears near the outlet region. The local profiles of catalytic combustion reaction rate of the four cases at the middle of the reforming catalyst layer are exhibited in Figure 16. The profiles of the reaction rate are significantly affected by the distributions of the catalyst. The maximum reaction rates are 4276.0, 1215.4, 1888.6 and 3052.1 mol/(m³ s), respectively. The reaction rate of Cases A and D is directly decreased along the channel direction, while it is increased and then decreased for Cases B and C.

4. Conclusions

A two-dimensional model is developed to examine the heat and mass transport process in microchannel reactors for hydrogen production. In this study, a non-uniform catalyst

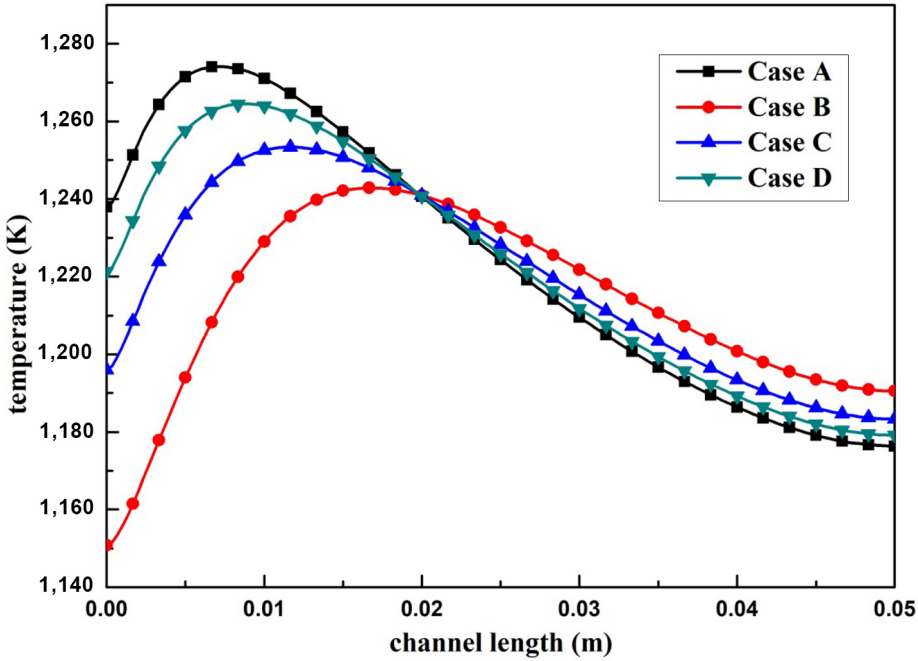
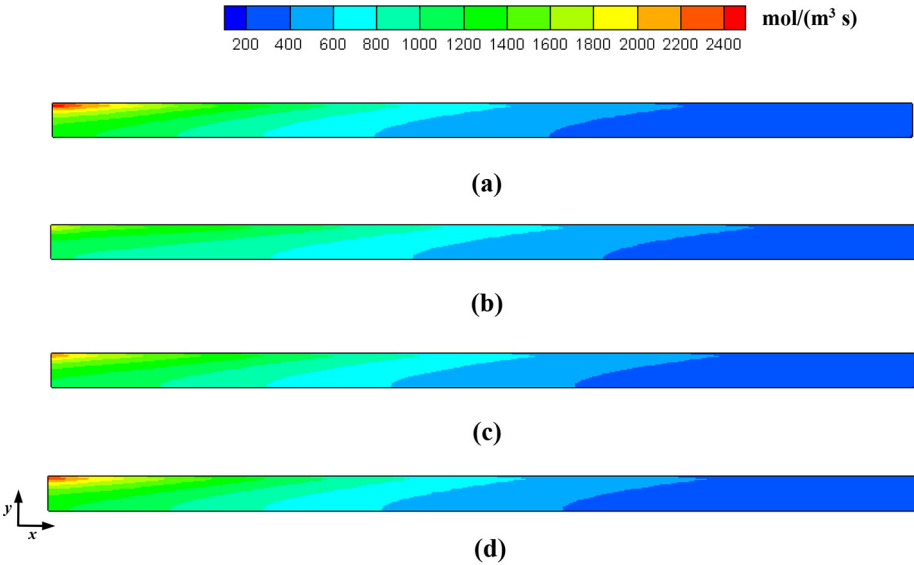


Figure 8. Temperature distributions at the middle of the solid plate of the four cases



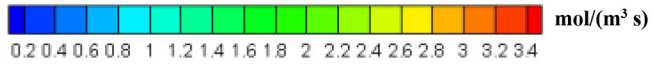
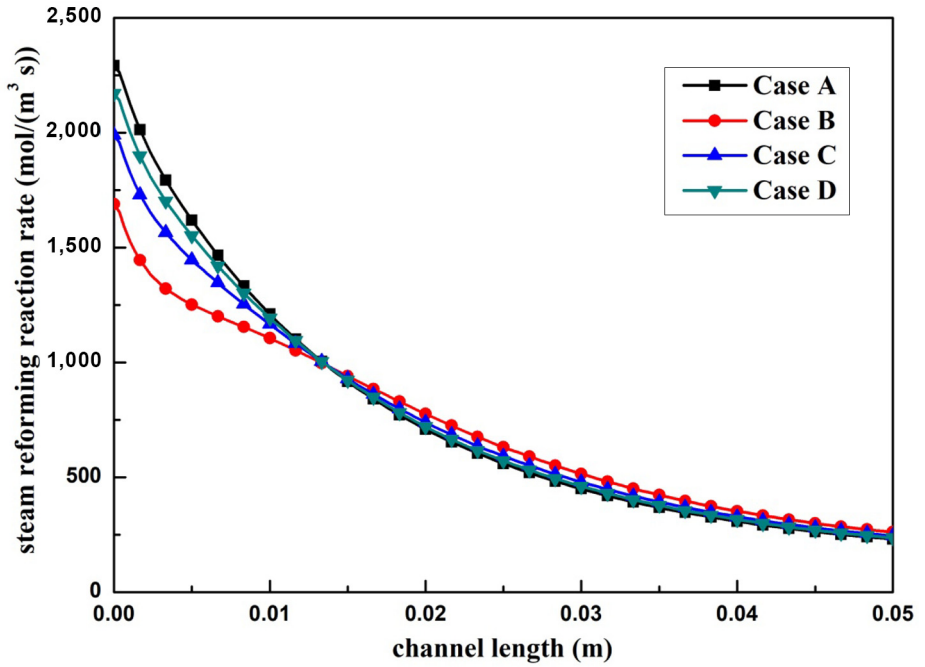
Notes: (a) Case A; (b) Case B; (c) Case C; (d) Case D

Figure 9. Steam reforming reaction rate distributions in the reforming catalyst layer of the four cases

HFF
32,10

3204

Figure 10.
Steam reforming
reaction rate of the
four cases at the
middle of the
reforming catalyst
layer



(a)



(b)



(c)



(d)

Figure 11.
Water-gas shift
reaction rate
distributions in the
reforming catalyst
layer of the four cases

Notes: (a) Case A; (b) Case B; (c) Case C; (d) Case D

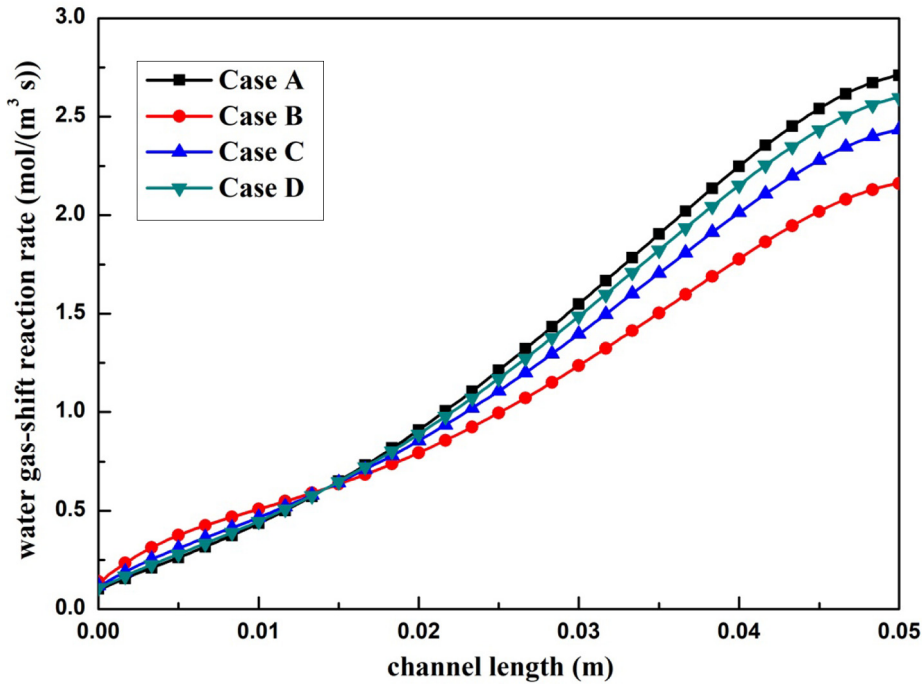


Figure 12. Water-gas shift reaction rate of the four cases at the middle of the reforming catalyst layer

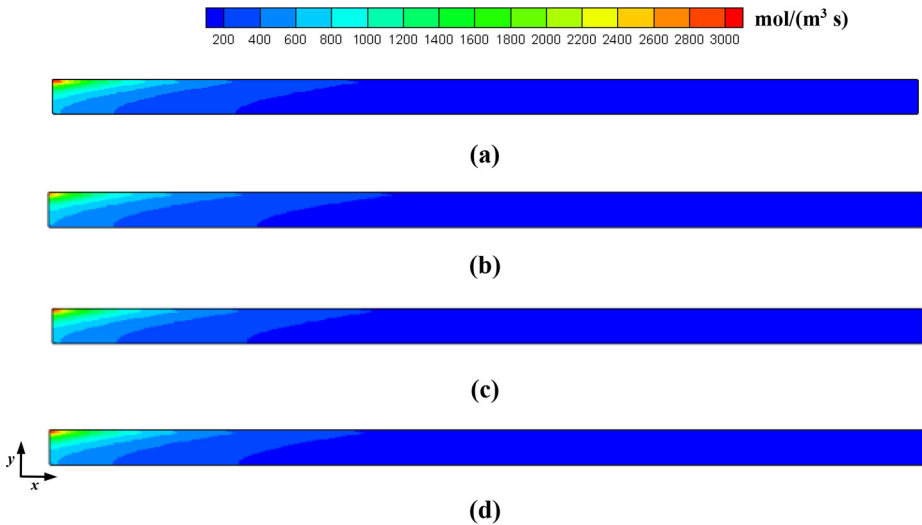


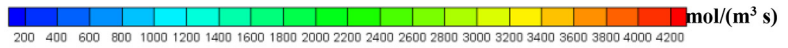
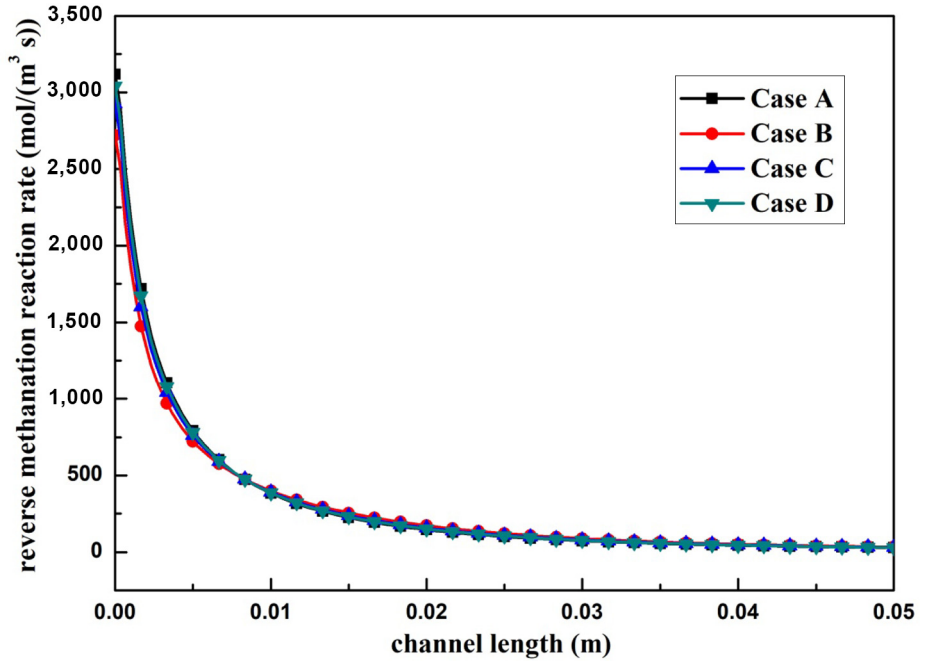
Figure 13. Reverse methanation reaction rate in the reforming catalyst layer of the four cases

Notes: (a) Case A; (b) Case B; (c) Case C; (d) Case D

HFF
32,10

3206

Figure 14.
Reverse methanation
reaction rate of the
four cases at the
middle of the
reforming catalyst
layer



(a)



(b)



(c)



(d)

Figure 15.
Catalytic combustion
reaction rate
distributions in the
combustion catalyst
layer of the four cases

Notes: (a) Case A ;(b) Case B; (c) Case C; (d) Case D

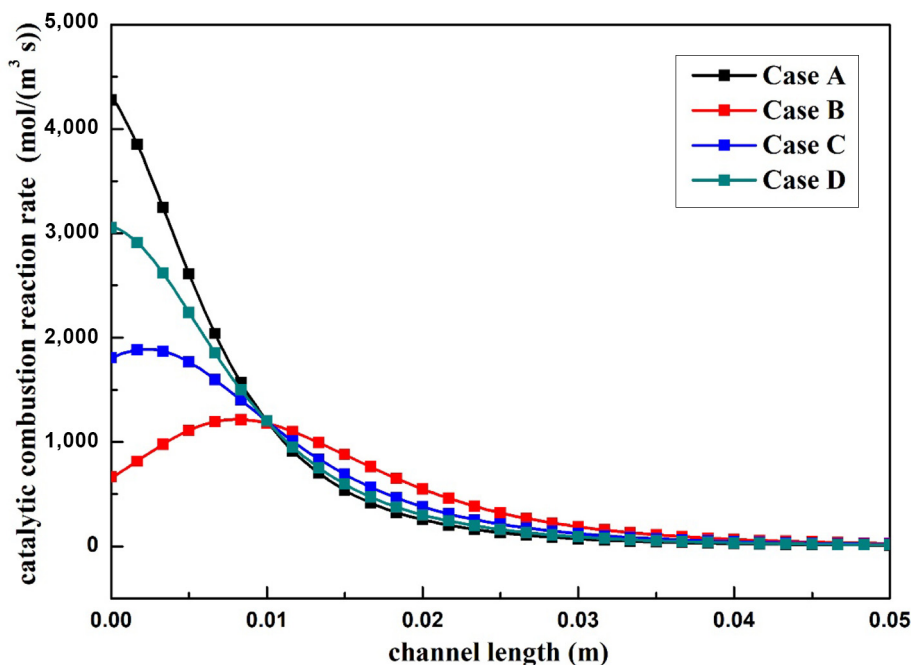


Figure 16. Catalytic combustion reaction rate of the four cases at the middle of the reforming catalyst layer

distribution is applied in the combustion catalyst layer of microchannel reactors to minimize the temperature. The mass transfer and chemical kinetics processes in the reactors are also influenced due to the non-uniform catalyst distribution in the combustion side. It is found that the maximum temperature of Cases B, C and D is greatly reduced compared to Case A and the location of the maximum temperature is also affected by the catalyst distribution. It is concluded that the maximum temperature inside the reactor can be reduced by means of the non-uniform catalyst distribution in the combustion catalyst layer with only a slight methane conversion penalty.

References

- Bartholomew, C.H. (2001), "Mechanisms of catalyst deactivation", *Applied Catalysis A: General*, Vol. 212 Nos 1/2, pp. 17-60.
- Bhat, S.A. and Sadhukhan, J. (2009), "Process intensification aspects for steam methane reforming: an overview", *AIChE Journal*, Vol. 55 No. 2, pp. 408-422.
- Chen, Z., Ingham, D., Ismail, M., Ma, L., Hughes, K.J. and Pourkashanian, M. (2020), "Effects of hydrogen relative humidity on the performance of an air-breathing PEM fuel cell: a numerical study", *International Journal of Numerical Methods for Heat and Fluid Flow*, Vol. 30 No. 4, pp. 2077-2097.
- Elnashaie, S.S.E.H., Adris, A.M., Alubaid, A.S. and Soliman, M.A. (1990), "On the non-monotonic behavior of methane steam reforming kinetics", *Chemical Engineering Science*, Vol. 45 No. 2, pp. 491-501.

- Irani, M., Alizadehdakheel, A., Pour, A.N., Hoseini, N. and Adinehnia, M. (2011), "CFD modeling of hydrogen production using steam reforming of methane in monolith reactors: surface or volume-base reaction model", *International Journal of Hydrogen Energy*, Vol. 36 No. 24, pp. 15602-15610.
- Jeon, S.W., Yoon, W.J., Baek, C. and Kim, Y. (2013), "Minimization of hot spot in a microchannel reactor for steam reforming of methane with the stripe combustion catalyst layer", *International Journal of Hydrogen Energy*, Vol. 38 No. 32, pp. 13982-13990.
- Li, S.A. and Sunden, B. (2018), "Effect of gas diffusion layer deformation on the transport phenomena and performance of PEM fuel cells with interdigitated flow fields", *International Journal of Hydrogen Energy*, Vol. 43 No. 33, pp. 16279-16292.
- Li, S.A., Yuan, J.L., Xie, G.N. and Sunden, B. (2017), "Numerical investigation of transport phenomena in high temperature proton exchange membrane fuel cells with different flow field designs", *Numerical Heat Transfer A*, Vol. 72 No. 11, pp. 807-820.
- Li, S.A., Peng, C.D., Shen, Q.W., Wang, C.Y., Cheng, Y.Z. and Yang, G.G. (2021), "Impact of membrane phosphoric acid doping level on transport phenomena and performance in high temperature PEM fuel cells", *Membranes*, Vol. 11 No. 11, p. 817.
- Mauro, A., Arpino, F., Massarotti, N. and Nithiarasu, P. (2010), "A novel single domain approach for numerical modelling solid oxide fuel cells", *International Journal of Numerical Methods for Heat and Fluid Flow*, Vol. 20 No. 5, pp. 587-612.
- Mundhwa, M. and Thurgood, C.P. (2017), "Numerical study of methane steam reforming and methane combustion over the segmented and continuously coated layers of catalysts in a plate reactor", *Fuel Processing Technology*, Vol. 158, pp. 57-72.
- Ni, M. (2013), "2D heat and mass transfer modeling of methane steam reforming for hydrogen production in a compact reformer", *Energy Conversion and Management*, Vol. 65, pp. 155-163.
- Peng, Y., Bahrami, G., Khodadadi, H., Karimi, A., Soleimani, A., Karimipour, A. and Rostami, S. (2020), "Three dimensional numerical simulation of polymer electrolyte membrane fuel cell", *International Journal of Numerical Methods for Heat and Fluid Flow*, Vol. 30 No. 1, pp. 427-451.
- Settar, A., Nebbali, R., Madani, B. and Abboudi, S. (2015), "Numerical investigation on the wall-coated steam methane reformer improvement: effects of catalyst layer patterns and metal foam insertion", *International Journal of Hydrogen Energy*, Vol. 40 No. 29, pp. 8966-8979.
- Shen, Q.W., Li, S.A., Yang, G.G., Huang, N.B., Yuan, J.L. and Sunden, B. (2019), "Analysis of heat and mass transport characteristics in anode-supported solid oxide fuel cells at various operating conditions", *Numerical Heat Transfer A*, Vol. 75 No. 8, pp. 509-522.
- Sohn, S., Baek, S.M., Nam, J.H. and Kim, C. (2016), "Two-dimensional micro/macroscale model for intermediate temperature solid oxide fuel cells considering the direct internal reforming of methane", *International Journal of Hydrogen Energy*, Vol. 41 No. 12, pp. 5582-5597.
- Song, X., Williams, W.R., Schmidt, L.D. and Aris, R. (1991), "Ignition and extinction of homogeneous-heterogeneous combustion: CH₄ and C₃H₈ oxidation on Pt", *Symposium (International) on Combustion*, Vol. 23 No. 1, pp. 1129-1137.
- Wang, F., Zhou, J. and Wang, G.Q. (2012), "Transport characteristic study of methane steam reforming coupling methane catalytic combustion for hydrogen production", *International Journal of Hydrogen Energy*, Vol. 37 No. 17, pp. 13013-13021.
- Wang, H., Yang, G.G., Li, S.A., Shen, Q.W., Li, Z. and Chen, B.J. (2021), "Numerical study on the effect of discrete catalytic layer arrangement on methane steam reforming performance", *RSC Advances*, Vol. 11 No. 5, pp. 2958-2967.
- Xu, J. and Froment, G.F. (1989), "Methane steam reforming, methanation and water gas shift: I intrinsic kinetics", *AIChE Journal*, Vol. 35 No. 1, pp. 88-96.

Yuan, J.L., Ren, F. and Sunden, B. (2007), "Analysis of chemical reaction coupled mass and heat transport phenomena in a methane reformer duct for PEMFCs", *International Journal of Heat and Mass Transfer*, Vol. 50 Nos 3/4, pp. 687-701.

Zanfir, M. and Gavriilidis, A. (2003), "Catalytic combustion assisted methane steam reforming in a catalytic plate reactor", *Chemical Engineering Science*, Vol. 58 No. 17, pp. 3947-3960.

Zanfir, M. and Gavriilidis, A. (2004), "Influence of flow arrangement in catalytic plate reactors for methane steam reforming", *Chemical Engineering Research and Design*, Vol. 82 No. 2, pp. 252-258.

Corresponding author

Bengt Ake Sunden can be contacted at: bengt.sunden@energy.lth.se